
Synthetic data generation method for hybrid image–tabular data using two generative adversarial networks

Tomohiro Kikuchi (1,2), Shouhei Hanaoka (3), Takahiro Nakao (1), Tomomi Takenaga (3)
Yukihiro Nomura (1,4), Harushi Mori (2), Takeharu Yoshikawa (1)

1 Department of Computational Diagnostic Radiology and Preventive Medicine, The University of Tokyo Hospital, Tokyo, Japan.

2 Department of Radiology, Jichi Medical University, School of Medicine, Tochigi, Japan.

3 Department of Radiology, The University of Tokyo Hospital, Tokyo, Japan.

4 Center for Frontier Medical Engineering, Chiba University, Chiba, Japan.

The generation of synthetic medical records using generative adversarial networks (GANs) has become increasingly important for addressing privacy concerns and promoting data sharing in the medical field. In this paper, we propose a novel method for generating synthetic hybrid medical records consisting of chest X-ray images (CXRs) and structured tabular data (including anthropometric data and laboratory tests) using an auto-encoding GAN (α GAN) and a conditional tabular GAN (CTGAN). Our approach involves training a α GAN model on a large public database (pDB) to reduce the dimensionality of CXRs. We then applied the trained encoder of the GAN model to the images in original database (oDB) to obtain the latent vectors. These latent vectors were combined with tabular data in oDB, and these joint data were used to train the CTGAN model. We successfully generated diverse synthetic records of hybrid CXR and tabular data, maintaining correspondence between them. We evaluated this synthetic database (sDB) through visual assessment, distribution of interrecord distances, and classification tasks. Our evaluation results showed that the sDB captured the features of the oDB while maintaining the correspondence between the images and tabular data. Although our approach relies on the availability of a large-scale pDB containing a substantial number of images with the same modality and imaging region as those in the oDB, this method has the potential for the public release of synthetic datasets without compromising the secondary use of data.

I. INTRODUCTION

Public availability of data is valuable not only for the reproducibility of research but also for the discovery of new knowledge through secondary analysis. However, sharing medical data is difficult because they contain sensitive personal information. To address this issue, synthetic data generation using generative models has gained attention as a privacy-preserving method for data sharing [1, 2]. By training the appropriate generative models based on the dataset, the model can create fully synthetic records with characteristics similar to those of the original dataset. Several generative adversarial network (GAN)-based methods have been proposed in medical research field to date [3–7].

In many real-world situations, including those in the medical field, data are not inherently of a single type, and it is reasonable to function with multiple types of data simultaneously. Functioning with hybrid data, which combine both image and tabular data into a single record, is important because it can provide more comprehensive insights for applications such as disease prognosis and personalized treatment planning. For example, in the context of COVID-19, hybrid data combining chest radiographs and laboratory values can enhance the predictive models for patient outcomes [8]. However, existing data synthesis methods in the medical field have primarily focused on generating either image data (such as CT and MRI scans) or tabular data (e.g., anthropometric data and medical test results, which are organized in tables or matrix formats) and have not been able to generate both simultaneously.

Generating synthetic hybrid data has been challenging, primarily because of technical limitations such as the curse of dimensionality, wherein handling high-dimensional data from images and combining them with tabular data is computationally intensive and complex. In this paper, we present a breakthrough approach for generating synthetic hybrid data by effectively addressing these technical barriers. With our approach, the sharing of hybrid data becomes more common, opportunities to gain new insights through comprehensive secondary analyses using such data are likely to increase. Our method involves performing dimensionality reduction on images from a hybrid dataset to obtain latent space vectors (hereafter referred to as image features) and then combining these with the corresponding tabular data to create an integrated dataset. This dataset can then be used as input for a generative model designed for tabular data. Using two GANs (auto-encoding GAN (α GAN) [9] and conditional tabular GAN (CTGAN) [10]), we created synthetic hybrid records. In this study, the Radiological Society of North America (RSNA) Pneumonia Detection Challenge dataset [11] (a publicly available CXRs dataset) was used for α GAN model pretraining, and then synthetic records that mimicked Stony Brook University Covid-19 Positive Cases [12,13] (a publicly available hybrid dataset which contains CXRs and tabular data) were generated using the trained α GAN and CTGAN.

Contribution of our Study

Several data generation studies have been conducted on images and tabular data, although techniques for generating synthetic hybrid records have not been developed. In contrast to previous research (discussed in Section II. RELATED WORKS), the contributions of this study are as follows:

- 1) We introduced a method capable of simultaneously generating synthetic records that contain both image and tabular data.
- 2) To achieve this, we devised a method to perform a dimensionality reduction of images from the original database using a pretrained GAN model, which was then concatenated with tabular data and input into the CTGAN. Notably, using the original hybrid dataset is not necessary for pretraining of α GAN model because another image dataset can be utilized, eliminating the need for a large size of the original dataset as the source for synthesis.
- 3) Consequently, with only 1,074 (training + validation) cases from original hybrid dataset, we successfully generated a synthetic hybrid database with intermediate-resolution (256×256 pixels) chest X-ray images (CXRs) and 70 tabular data items for each synthetic record.

II. RELATED WORKS

GAN, introduced by Goodfellow et al., has significantly contributed to the field of computer vision [14]. In the medical domain, GANs have been employed in a wide range of applications including modality transfer, hyperresolution, noise reduction, and synthetic medical record generation [4,15,16]. GANs are composed of two adversarial networks: a generator G and discriminator D . Given a set of real data samples x that originate from a true source distribution p_s , the generator G aims to produce synthetic samples that mimic this distribution. The generator consumes noise samples z , typically drawn from a Gaussian distribution, and maps these to synthetic data points. This transformation can be represented as $G : Z \rightarrow X_g$, where Z is the domain of the noise samples, and X_g is the set of generated samples. By contrast, discriminator D assesses the authenticity of the data samples. It accepts either a real data sample or a synthetic sample produced by G and outputs a probability score indicating the probability of the given sample to be real. This can be represented as $D: X' \rightarrow [0, 1]$, where X' is the combined set of real and generated data samples. Both the networks engage in a min-max game to learn the distribution \hat{p}_s that approximates p_s . In conditional GANs, additional input y is provided to both the generator and discriminator networks to control the output of the generator [17]. This additional input enables the generation of data with specific characteristics. The generator G function is

$G: Z \times Y \rightarrow X_g$, where Y is the set of conditions y . Similarly, the discriminator considers the y context when determining authenticity. The main objective of both networks in this setting is to learn and replicate the conditional distribution $p_{s|y}$. This enables the generation of highly specific data for specific applications. Previous studies on the synthesis of CXRs and tabular medical data using GANs are described in the following section.

A. Generation of CXRs

For synthetic CXRs generation, several studies using nonconditional GANs have been proposed [5,18–20]. These studies used at least 5840 images with a minimum input image size of 244×244 pixels to train the networks. This implies that a large number of CXRs are required to train GANs with intermediate–to high–resolution images. In another study, synthetic CXR generation using conditional GAN was performed with 1124 CXRs used for training, but with a smaller input size of 112×112 pixels because of the smaller image dataset [21]. All the aforementioned studies were intended for data augmentation.

B. Generation of medical tabular data

The application of GAN to tabular data began a few years after its application to images. Conditional GAN models include TGAN, TableGAN, CTGAN, MedGAN, CopulaGAN, and CTAB–GAN [2,10,22–24]. In studies using tabular data generation for augmentation in the medical field, no architecture exists that can demonstrate superiority in all tasks; however, the performance of the CTGAN model seems to be stable [6,24,25].

III. MATERIALS AND METHODS

We generated synthetic records in three steps: 1) pretraining of α GAN model using a large image database (hereafter referred to as a public database or pDB, emphasizing that acquiring such databases has become relatively effortless); 2) training the CTGAN model on a hybrid database (defined as the original database or oDB, which, for the purposes of this study, is assumed to be a private dataset that cannot be shared) after dimensionality reduction of its images using the encoder of α GAN model; and 3) generation of synthetic medical records using the trained generators of CTGAN and α GAN models (defined as synthetic database or sDB) (Figures 1–3). To compare our experimental method, we also created a group of cases in which the image features and tabular data did not match (defined as an unmatched database or uDB) (Figure 3).

A. Datasets and preprocessing

Considering a large number of images to be necessary for the training of α GAN model with intermediate–level images, we used the RSNA Pneumonia Detection Challenge dataset [11] as pDB. This dataset consists of approximately 30,000 frontal–view CXRs. In this study, we used a subset of this dataset consisting of 29,684 valid CXRs, excluding cases with invalid views (e.g., lateral or abdominal views). We randomly divided 29,684 CXRs into a training dataset (80%) and a validation dataset (20%). In addition, we used Stony Brook University Covid–19 Positive Cases [12,13] as oDB. This hybrid database comprises 1384 COVID–19 positive cases, featuring diverse imaging modalities and comprehensive clinical tabular data. It was designed to facilitate the development of artificial intelligence systems for diagnostic and prognostic modeling. We used 1343 cases with both CXR and corresponding tabular data. Originally, the tabular data had 84 variables per case, and we removed duplicates or similar items, resulting in a final set of 70 items (the list of items used for the analysis is described in Appendix 1). We randomly split the oDB into training, validation, and test datasets in a ratio of 6:2:2. Categorical variables with an inherent order were coded based on their order, with missing values coded as one unit greater than the highest order. Categorical variables with an inherent order were coded based on their order using continuous integers starting from zero, with missing values coded as one unit greater than the highest order. Unordered categorical variables were also coded in

alphabetical sequences using continuous integers starting from zero, and missing values were assigned a subsequent integer. Missing numerical variables were imputed using mean values from the training set. All images in the pDB and oDB were resized to 256×256 pixels before being input into the networks.

B. Networks

We adopted α GAN as a network to compress the image dimensions. α GAN is a structure that combines variational auto-encoders (VAE) [26] with GAN and has been reported to produce sharper images than VAE while enabling the acquisition of latent variables that follow a Gaussian distribution similar to VAE [9,27]. We constructed network with reference to a study adapting α GAN to intermediate-resolution CXRs [28] (Appendix 2).

We adopted the CTGAN as the network for synthetic tabular data generation. The CTGAN is a GAN-based method for modeling the distribution of tabular data. It performs normalization on each column of complex data distributions with respect to categorical variables, and trains the model using a conditional generator and discriminator [10]. We used the standalone library of the CTGAN ver. 0.7.0 (<https://github.com/sdv-dev/CTGAN>).

C. Training

First, we performed α GAN model training using images from the pDB (Figure 1). The image input to the network was 256×256 pixels and the number of latent vectors was set to 128 (i.e., one image was converted to 128 image features). Subsequently, we trained the CTGAN model on oDB, which served as the source of the synthetic hybrid records (Figure 2). After adapting the trained encoder of α GAN model to the images in the oDB and obtaining the encoded image features, we combined these image features with tabular data from the oDB and trained the CTGAN model using the combined data.

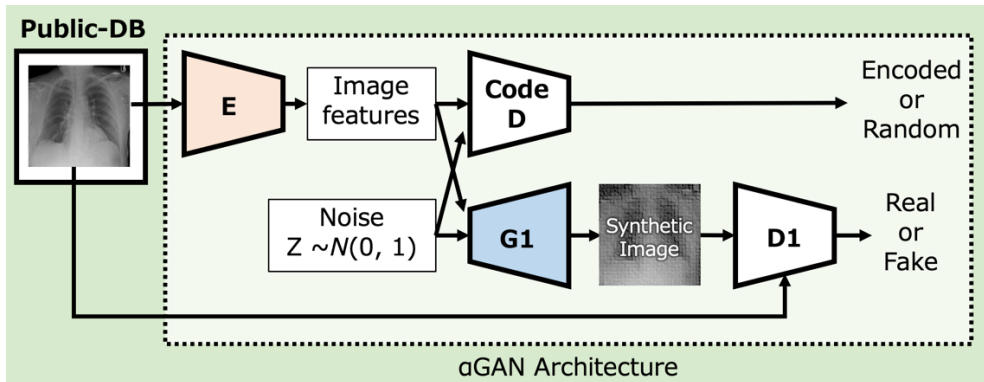


Figure 1. Training of auto-encoding GAN (α GAN). As a pretraining step for applying the α GAN to the original database, the network was trained on a public database. Encoder (E): It accepts real images and encodes them into a latent code representing a compressed representation of the input images. Generator (G1): The latent codes generated by E are used to produce fake (generated) images that resemble real images. Discriminator (D1): It determines whether an image is real (from the dataset) or fake (generated by G1). Code discriminator (Code D): It differentiates between real latent codes (sampled from a Gaussian distribution) and fake latent codes (generated by E). The trained E was used for dimension reduction, as shown in Figure 2, whereas the trained G1 was reused for image reconstruction, as shown in Figure 3.

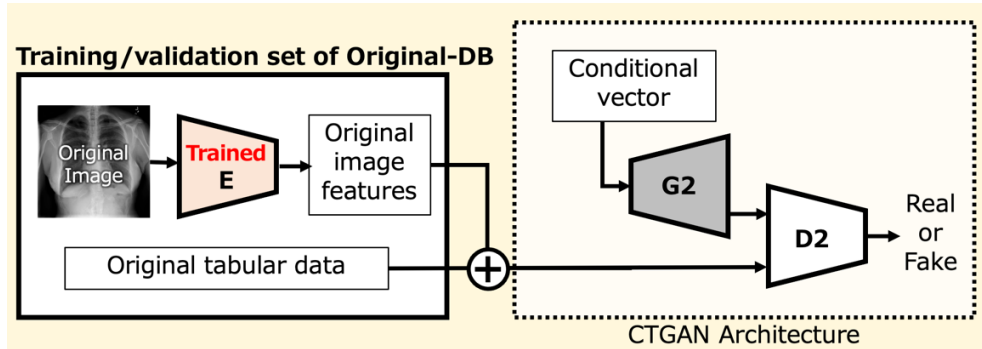


Figure 2. Training of conditional tabular GAN (CTGAN). In this step, using the trained auto-encoding GAN encoder (Trained E), we first performed a dimensionality reduction of the images in the training and validation sets of the original database into image features. These image features were then combined with tabular data, and the combined data were used for the CTGAN training. The generator of the CTGAN (G2) was trained to output fake data that mimicked the combined data from the original database. G2 is reused in the data-generating step (Figure 3).

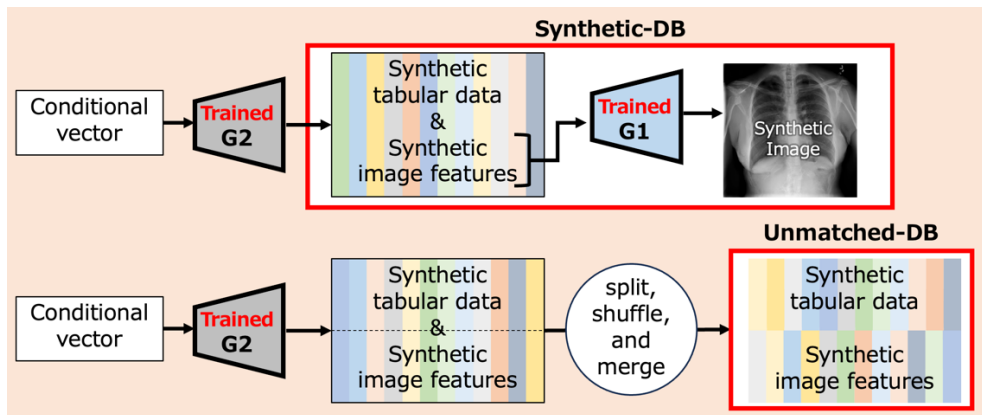


Figure 3. Synthetic Hybrid data generation. Using the trained generator of conditional tabular GAN (Trained G2), we can generate a set of synthetic tabular data and image features based on a conditional vector. A synthetic image can also be generated by passing the image features from the generated record through the trained generator of auto-encoding GAN (G1). The database created in this process is defined as a synthetic database. In addition, we split the output of the trained G2 into tabular data and image features, shuffled their order, and merged them. We defined this database as an unmatched database.

D. Synthetic hybrid data generation

Using the trained generator of the CTGAN model (Trained G2 in Figure 3), we obtained synthetic records as combined data containing image features and tabular data (Figure 3). Image reconstruction can be performed by passing the synthetic image features to the trained generator of aGAN model (Trained G1 in Figure 3). We created 40,000 synthetic records as the sDB and adjusted the frequencies of the categorical variable combinations to match those of the oDB. From these 40,000 records, we randomly selected the numbers required for our evaluation methods and used them in our analysis. In addition, we prepared an unmatched database (uDB) as a benchmark for comparison with the proposed method. The uDB was also generated using the trained generator of the CTGAN (Trained G2); however, we split the generated data into tabular and image feature components, shuffled them, and merged them. Consequently, the uDB was formed with no correspondence between the tabular and image components (Figure 3). Similar to the sDB, 40,000 instances were generated for the uDB.

E. Evaluation methods

First, we visually confirmed that images interpreted as CXRs were generated in the sDB. Subsequently, the following three aspects were evaluated:

1. Distribution of interrecord distances

We numerically confirmed that the generated cases did not experience mode collapse, which is a common problem associated with GAN use. For each database, we standardized the values in each column (both tabular data and image features) of the records and computed the Euclidean distances between distinct pairs within the dataset. For oDB, we utilized 1,074 (total training and validation) cases for the calculation. For the sDB and uDB, we randomly sampled 1,074 cases from each database and performed the same calculations.

2. Visualization of similarity between datasets

To visualize the similarities among the datasets, we employed t-stochastic neighbor embedding (SNE) plots [29,30]. We combined all subset records used in Subsection “Distribution of interrecord distances” in the data frame. We then created a two-dimensional t-SNE plot to visualize the differences in distribution among the three groups of records. The t-SNE implementation was performed using the Sci-kit learn library.

3. Usability

We assessed usability by evaluating the accuracy of a classification model trained using the generated records (sDB or uDB) and tested it on test cases from oDB. The independent variable was the clinical course (discharge or deceased), and the other 197 variables (69 from tabular data and 128 from image features) were used as the independent variables. LightGBM was used as our evaluation model (<https://github.com/microsoft/LightGBM>) and tested three different input types for the analysis: image features only, tabular data only, and a combination of both. The model was evaluated by using the area under the receiver operating characteristic curve (AUC). We varied the number of training-generated records to 100, 1000, 5000, 10000, and 15000, and plotted the performance. We set the LightGBM hyperparameters as follows: max depth = 5, num_boost_round = 1000, and early stopping rounds = 100, while maintaining the default values for the remaining parameters. These settings were consistent across all runs, and we conducted ten trials for each varying number of sDB records.

IV. EVALUATION RESULTS

Figure 4 shows 12 generated images randomly selected from the sDB. These images demonstrate the diversity achieved using the proposed approach. In Appendix 3, we present the synthetic CXRs for four cases of normal BMI (18.5–25) and severe obesity (BMI > 40) from the sDB dataset.

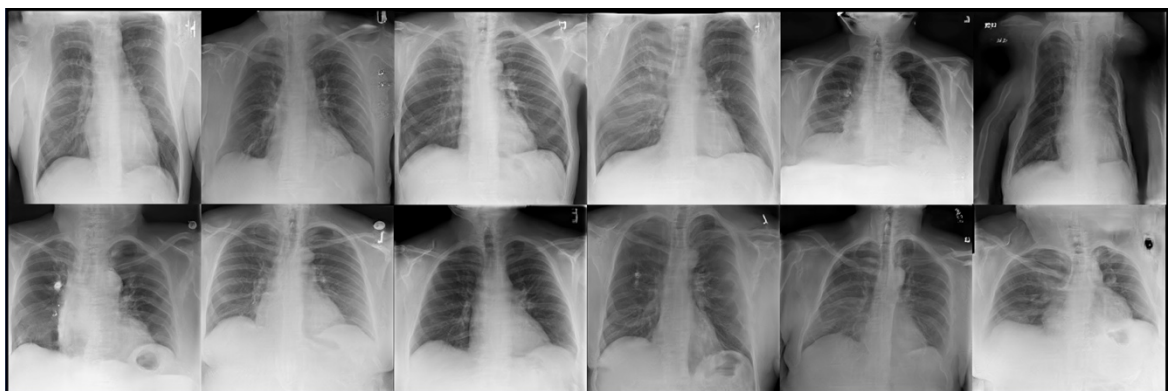


Figure 4. Chest X-ray images of 12 randomly selected cases from synthetic database. The images were generally of good quality and variety, but broken images were also produced, such as the two on the far-right side.

	oDB	sDB	uDB
Distance between two records (Median [interquartile range])	13.8 [12.0, 15.9]	15.5 [14.2, 17.1]	15.5 [14.2, 16.9]

Table 1. Interrecord distances in each database.

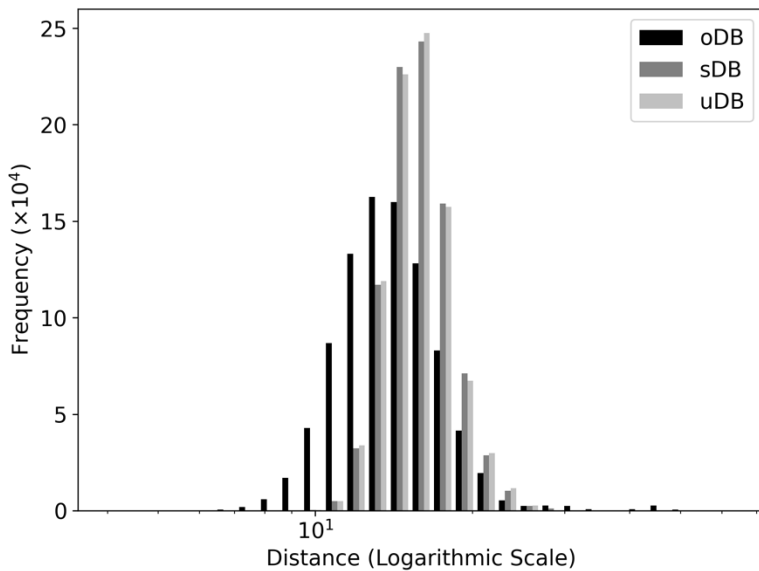


Figure 5. Histogram of interrecord distances. The x-axis is on a logarithmic scale, and the bins are divided according to logarithmic values. oDB: original database, sDB: synthetic database, uDB: unmatched database

Table 1 lists the median and quartiles of the distances between records for each dataset, and Figure 5 shows a histogram. The distribution of the interrecord distance of the sDB was not near zero (sDB: 13.8 [12.0, 15.9]. cf. oDB: 15.5 [14.2, 17.1]). This indicated that the sDB did not generate only similar records. The distributions of sDB and uDB were nearly the same, and the inconsistencies between the tabular data and images did not appear numerically.

When performing a t-SNE plot, there seemed to be some bias owing to the dataset in certain areas; however, the overlap between the oDB and sDB appears to be reasonably good (Figure 6). Using this method, sDB and uDB also exhibited similar characteristics.

Table 2 and Figure 7 show the results of the classification of clinical outcomes. Models trained on oDB including tabular data resulted in a good AUC of approximately 0.9, whereas those using only image features produced an AUC of 0.57. This suggests that predictions based solely on the images are challenging. Using the sDB for training, when tabular data were included in the input, the results were similar to those obtained using the oDB. Furthermore, including only image features from the sDB led to a performance equivalent to or better than that of the oDB. Increasing the number of records improved performance but plateaued at approximately 5000 records. As expected, the AUC was approximately 0.5 when using only image features with uDB. When tabular data were included for classification, because the integrity of the tabular data in the uDB was preserved, the AUCs were nearly equivalent to the results obtained with the sDB.

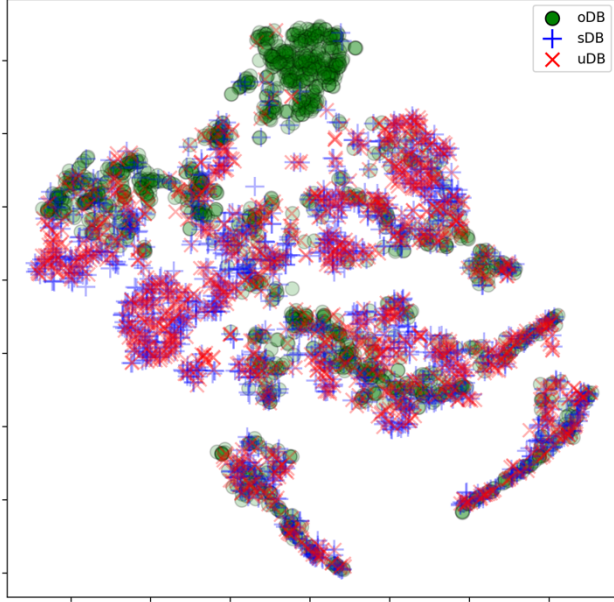


Figure 6. Two-dimensional plot based on t-Stochastic Neighbor Embedding. Cases from the original database are shown in green, those from the synthetic database in blue, and those from the unmatched database in red.
oDB: original database, sDB: synthetic database, uDB: unmatched database

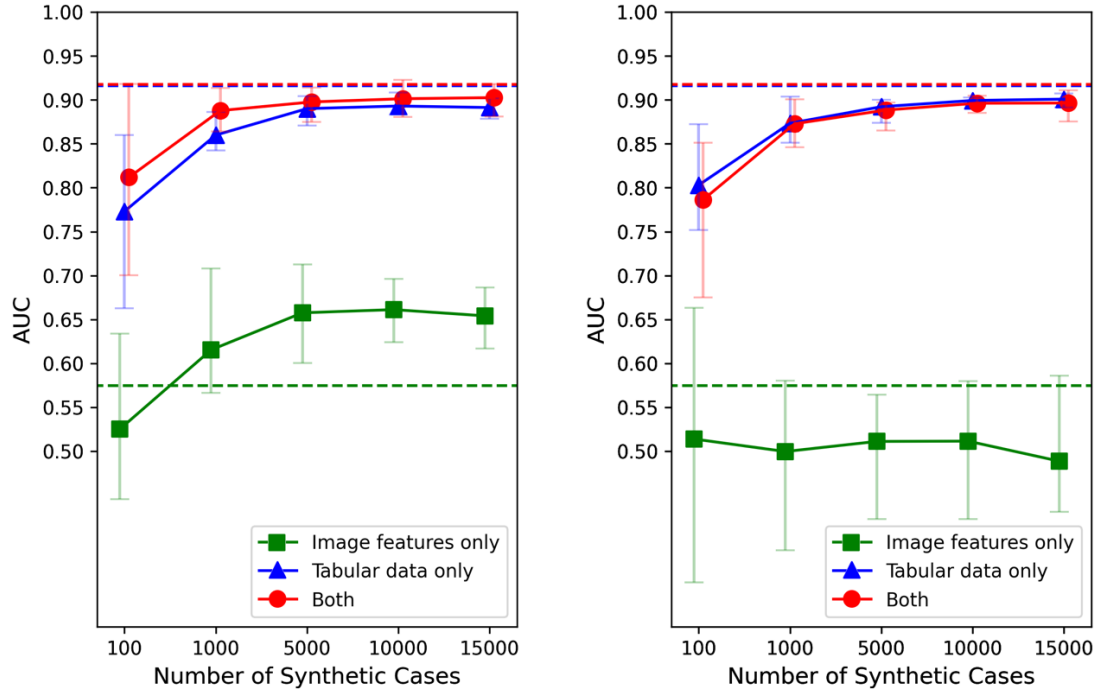


Figure 7. Classification results of clinical course. The left figure shows training with records in the synthetic database (sDB), and the right figure shows training with records in the unmatched database (uDB). The solid lines represent those trained with sDB or uDB and tested with test cases from the original database (oDB). The upper and lower ends of the whiskers represent the maximum and minimum values of the ten trials, respectively. The dashed lines are both trained in the training and validation cases in the oDB as well as tested in the test cases in the oDB and are shown for reference. For "both" and "tabular data only," the prediction accuracy was high. For "image features only," the performance was moderate when trained on sDB, and the scores could be better than that of oDB. By contrast, in the case of "image features only" in uDB, the AUC remained approximately 0.5 because of the unmatched image features and clinical outcomes.

		oDB	sDB	uDB
Classification performance to test cases from oDB (AUC)	Image features	0.57	0.53 – 0.66	0.49 – 0.51
	Tabular data	0.92	0.77 – 0.89	0.80 – 0.90
	Both	0.92	0.85 – 0.91	0.79 – 0.89

Table 2. Classification performance to test cases from oDB

V. DISCUSSION

In this study, we proposed a novel approach by training an architecture capable of dimensionality reduction (in this study, α GAN) on a large pDB, compressing the dimensions of oDB images through this model and passing them through a tabular-compatible GAN (in this study, CTGAN). We successfully generated synthetic records of hybrid CXR and tabular data while maintaining the correspondence between them. The records generated using our method are diverse and can contribute to various secondary analyses. To the best of our knowledge, this is the first study to simultaneously generate hybrid CXR and medical tabular data. GANs are used to generate virtual patient cases for two distinct purposes: data augmentation and data sharing [2,4,5,16,22]. For augmentation, generating a subset of the database using the information required to solve a predetermined task is sufficient. However, for data sharing, synthetic records that mimic all variables and their characteristics in the original database maximize the potential for secondary analyses. However, training GANs on a database containing high-dimensional data is challenging if the database is not large, and the datasets collected by medical researchers are generally not large. To address this difficulty, we devised a method to effectively reduce the dimensionality of images by training the α GAN model on another image dataset. We then combined the latent vectors with tabular data and trained the CTGAN model on the joint data. Consequently, we successfully created synthetic records containing intermediate-resolution CXRs and a large amount of tabular data from 1074 training-validation datasets, which is a relatively small number of records for training GANs for intermediate-resolution image generation [5,18–20].

From Table 1, we can conclude that a mode collapse does not occur. However, we can also observe broken images at low frequencies, indicating that not all the records in the dataset are perfect. In Figure 5, the peak of the sDB is to the right of the oDB peak, suggesting that there are fewer similar record pairs in the sDB. This can also be considered as one piece of evidence supporting the absence of model collapse. In the t-SNE plot in Figure 5, although the overlap between sDB and oDB is deemed good, some areas exist where they slightly diverge. Notably, the collective characteristics of the included data might differ slightly from those of the oDB. Furthermore, as both metrics showed similar characteristics between the uDB and sDB, it became clear that they were not effective metrics for evaluating the differences in these datasets (i.e., the inconsistency between the tabular data and image features). Future studies should focus on establishing useful metrics for evaluating and comparing datasets.

In addition, we performed clinical course classification (deceased or discharged) on the test datasets of the oDB using the sDB as the training dataset. When both image features and tabular data were used, the performance of the classification trained using the sDB approaches was reasonably close to that achieved using training data from the oDB, suggesting that the sDB captures the features of the oDB. Thus, sDB successfully imitated the features of oDB. In the case of utilizing image features only, sDB demonstrated a performance comparable to oDB when equal quantities of cases were used (AUC = 0.62 when the number of synthetic cases was 1,000, compared to AUC = 0.57 for oDB) (Figure 7).

Conversely, with uDB, the performance essentially degraded to random guessing when only image features were used. This contrast suggests that the sDB model could correctly align and generate images and tabular data. Moreover, as the number of cases in the sDB increased, its performance surpassed that of the oDB, illustrating the successful implementation of data augmentation using our implementation model.

Sharing medical data is valuable and important for ensuring the reproducibility of research and obtaining new insights through secondary analysis. However, the public release of the entire database is not easy because of privacy concerns. Reducing the number of items or categorizing continuous values into discrete values can be used to address privacy protection; however, such processing may compromise the secondary use of data. Our method can generate synthetic records for all items, including images and is considered to have high secondary usability while considering privacy.

One limitation of our method is that it relies on the availability of a large-scale pDB containing a substantial number of images of the same modality and imaging range as those in the oDB, which can be used to train the α GAN model. If the oDB itself is sufficiently large, the learning process of α GAN model using the pDB can be replaced by the oDB. However, because oDB, the dataset collected by medical researchers, is generally not large, and the expectation that the number and size of public databases will continue to increase in the future, we assumed the availability of a separate large image pDB. Additionally, a significant potential competitor to our research is the language learning model (LLMs). Recent advances in LLMs have enabled these systems to handle multimodal inputs [31,32]. This capacity to manage and manipulate abstract information within the latent space overlaps with the objectives of our current methodology to a certain extent. However, our approach distinctly focuses on the generation of synthesized data that closely aligns with the characteristics of the original data. This targeted outcome distinguishes the proposed method and demonstrates its unique value. Although both LLMs and our technique share a common underpinning in the form of advanced learning mechanisms, their roles remain divergent because of their differentiated goals. As the field continues to evolve, we anticipate that the functionalities of these two methodologies will retain their individuality and serve complementary roles in various applications.

future works

Application to data augmentation. Although this study focuses on the publication of a dataset, the proposed framework can also be used for data augmentation.

Extension to 3-Dimensional images. CXRs were used in this study. If this method could be extended to 3-Dimensional images such as CT images, it could demonstrate further usefulness.

Introducing a more rigorous privacy concept. In privacy research, GAN outputs may contain information from the original data. The concept of differential privacy (DP), which was developed in recent years, addresses this issue [33]. DP can be applied to the proposed method to ensure robust privacy.

limitations

First, in our implementation, we used α GAN and CTGAN; however, it was possible to replace them with other networks. We did not evaluate the way the performance changes when the architectures are replaced. We referred to previous studies on α GAN and CTGAN for medical records and selected them for the proposed method. Second, the minimum number of records in pDB and oDB and the maximum number of columns in oDB required to generate meaningful sDB are unknown. Our experimental results serve as indicators. Third, we used the default parameters of the lightGBM for classification and did not perform an optimal parameter search. Our study prioritizes simplicity and comparability over the establishment of better classification models. The performance could be improved by adjusting the parameters.

VI. CONCLUSION

Using α GAN and CTGAN models, we generated synthetic hybrid records consisting of intermediate-resolution CXRs and tabular data with 70 variables. Although we assumed the availability of another large-scale image database, the proposed method enables the creation of highly reusable synthetic hybrid data without releasing the original hybrid database.

ACKNOWLEDGMENT

This study was partially supported by the JST CREST, grant number JPMJCR21M2.

REFERENCES

- [1] J. Ficek, W. Wang, H. Chen, G. Dagne, and E. Daley, “Differential privacy in health research: A scoping review,” *J. Am. Med. Inform. Assoc.*, vol. 28, no. 10, pp. 2269–2276, Sep. 2021.
- [2] Z. Zhao, A. Kunar, R. Birke, and L. Y. Chen, “CTAB-GAN: Effective Table Data Synthesizing,” in *Proceedings of The 13th Asian Conference on Machine Learning*, 17–19 Nov 2021, vol. 157, pp. 97–112.
- [3] V. Bhagat and S. Bhaumik, “Data Augmentation using Generative Adversarial Networks for Pneumonia classification in chest Xrays,” in *2019 Fifth International Conference on Image Information Processing (ICIIP)*, 2019, pp. 574–579.
- [4] A. Goncalves, P. Ray, B. Soper, J. Stevens, L. Coyle, and A. P. Sales, “Generation and evaluation of synthetic patient data,” *BMC Med. Res. Methodol.*, vol. 20, no. 1, p. 108, May 2020.
- [5] D. Srivastav, A. Bajpai, and P. Srivastava, “Improved Classification for Pneumonia Detection using Transfer Learning with GAN based Synthetic Image Augmentation,” in *2021 11th International Conference on Cloud Computing, Data Science & Engineering (Confluence)*, 2021, pp. 433–437.
- [6] M. A. B. Hameed and Z. Alamgir, “Improving mortality prediction in Acute Pancreatitis by machine learning and data augmentation,” *Comput. Biol. Med.*, vol. 150, p. 106077, Sep. 2022.
- [7] R. Osuala, K. Kushibar, L. Garrucho, A. Linardos, Z. Szafranowska, S. Klein, B. Glocker, O. Diaz, and K. Lekadir, “Data synthesis and adversarial networks: A review and meta-analysis in cancer imaging,” *Med. Image Anal.*, p. 102704, Nov. 2022.
- [8] W. Liang, J. Yao, A. Chen, Q. Lv, M. Zanin, J. Liu, S. Wong, Y. Li, J. Lu, H. Liang, G. Chen, H. Guo, J. Guo, R. Zhou, L. Ou, N. Zhou, H. Chen, F. Yang, X. Han, W. Huan, W. Tang, W. Guan, Z. Chen, Y. Zhao, L. Sang, Y. Xu, W. Wang, S. Li, L. Lu, N. Zhang, N. Zhong, J. Huang, and J. He, “Early triage of critically ill COVID-19 patients using deep learning,” *Nat. Commun.*, vol. 11, no. 1, p. 3543, Jul. 2020.
- [9] M. Rosca, B. Lakshminarayanan, D. Warde-Farley, and S. Mohamed, “Variational Approaches for Auto-Encoding Generative Adversarial Networks,” *arXiv [stat.ML]*, 15–Jun–2017.
- [10] L. Xu, M. Skoulikidou, A. Cuesta-Infante, and K. Veeramachaneni, “Modeling Tabular data using Conditional GAN,” *Adv. Neural Inf. Process. Syst.*, 2019.
- [11] G. Shih, C. C. Wu, S. S. Halabi, M. D. Kohli, L. M. Prevedello, T. S. Cook, A. Sharma, J. K. Amorosa, V. Arteaga, M. Galperin-Aizenberg, R. R. Gill, M. C. B. Godoy, S. Hobbs, J. Jeudy, A. Laroia, P. N. Shah, D. Vummidi, K. Yaddanapudi, and A. Stein, “Augmenting the National Institutes of Health Chest Radiograph Dataset with Expert Annotations of Possible Pneumonia,” *Radiology: Artificial Intelligence*, vol. 1, no. 1, p. e180041, Jan. 2019.
- [12] J. Saltz, M. Saltz, P. Prasanna, R. Moffitt, J. Hajagos, E. Bremer, J. Balsamo, and T. Kurc, “Stony brook university covid-19 positive cases [data set]. the cancer imaging archive.” 2021.
- [13] K. Clark, B. Vendt, K. Smith, J. Freymann, J. Kirby, P. Koppel, S. Moore, S. Phillips, D. Maffitt, M. Pringle, L. Tarbox, and F. Prior, “The Cancer Imaging Archive (TCIA): maintaining and operating a public information repository,” *J. Digit. Imaging*, vol. 26, no. 6, pp. 1045–1057, Dec. 2013.
- [14] I. Goodfellow, J. Pouget-Abadie, M. Mirza, B. Xu, D. Warde-Farley, S. Ozair, A. Courville, and Y. Bengio, “Generative Adversarial Nets,” *Adv. Neural Inf. Process. Syst.*, vol. 27, 2014.
- [15] P. M. Cheng, E. Montagnon, R. Yamashita, I. Pan, A. Cadrian-Chenevert, F. Perdigón Romero, G. Chartrand, S. Kadoury, and A. Tang, “Deep Learning: An Update for Radiologists,” *Radiographics*, vol. 41, no. 5, pp. 1427–1445, Sep. 2021.
- [16] Y. Chen, X.-H. Yang, Z. Wei, A. A. Heidari, N. Zheng, Z. Li, H. Chen, H. Hu, Q. Zhou, and Q. Guan, “Generative Adversarial Networks in Medical Image augmentation: A review,” *Comput. Biol. Med.*, vol. 144, p. 105382, May 2022.
- [17] M. Mirza and S. Osindero, “Conditional Generative Adversarial Nets,” *arXiv [cs.LG]*, 06–Nov–2014.

- [18] H. Salehinejad, E. Colak, T. Dowdell, J. Barfett, and S. Valaee, “Synthesizing Chest X-Ray Pathology for Training Deep Convolutional Neural Networks,” *IEEE Trans. Med. Imaging*, vol. 38, no. 5, pp. 1197–1206, May 2019.
- [19] P. Ganesan, S. Rajaraman, R. Long, B. Ghoraani, and S. Antani, “Assessment of Data Augmentation Strategies Toward Performance Improvement of Abnormality Classification in Chest Radiographs,” in *2019 41st Annual International Conference of the IEEE Engineering in Medicine and Biology Society (EMBC)*, 2019, pp. 841–844.
- [20] S. Motamed, P. Rogalla, and F. Khalvati, “Data augmentation using Generative Adversarial Networks (GANs) for GAN-based detection of Pneumonia and COVID-19 in chest X-ray images,” *Informatics in Medicine Unlocked*, vol. 27, p. 100779, Jan. 2021.
- [21] A. Waheed, M. Goyal, D. Gupta, A. Khanna, F. Al-Turjman, and P. R. Pinheiro, “CovidGAN: Data Augmentation Using Auxiliary Classifier GAN for Improved Covid-19 Detection,” *IEEE Access*, vol. 8, pp. 91916–91923, May 2020.
- [22] N. Park, M. Mohammadi, K. Gorde, S. Jajodia, H. Park, and Y. Kim, “Data synthesis based on generative adversarial networks,” *Proceedings VLDB Endowment*, vol. 11, no. 10, pp. 1071–1083, Jun. 2018.
- [23] K. Armanious, C. Jiang, M. Fischer, T. Küstner, T. Hepp, K. Nikolaou, S. Gatidis, and B. Yang, “MedGAN: Medical image translation using GANs,” *Comput. Med. Imaging Graph.*, vol. 79, p. 101684, Jan. 2020.
- [24] S. Bourou, A. El Saer, T.-H. Velivassaki, A. Voulkidis, and T. Zahariadis, “A Review of Tabular Data Synthesis Using GANs on an IDS Dataset,” *Information*, vol. 12, no. 9, p. 375, Sep. 2021.
- [25] A. J. Rodriguez-Almeida, H. Fabelo, S. Ortega, A. Deniz, F. J. Balea-Fernandez, E. Quevedo, C. Soguero-Ruiz, A. M. Wagner, and G. M. Callico, “Synthetic Patient Data Generation and Evaluation in Disease Prediction Using Small and Imbalanced Datasets,” *IEEE J Biomed Health Inform*, vol. PP, Aug. 2022.
- [26] D. P. Kingma and M. Welling, “Auto-Encoding Variational Bayes,” *arXiv [stat.ML]*, 20–Dec–2013.
- [27] G. Kwon, C. Han, and D.-S. Kim, “Generation of 3D brain MRI using auto-encoding generative adversarial networks,” in *Lecture Notes in Computer Science*, Cham: Springer International Publishing, 2019, pp. 118–126.
- [28] T. Nakao, S. Hanaoka, Y. Nomura, M. Murata, T. Takenaga, S. Miki, T. Watadani, T. Yoshikawa, N. Hayashi, and O. Abe, “Unsupervised Deep Anomaly Detection in Chest Radiographs,” *J. Digit. Imaging*, vol. 34, no. 2, pp. 418–427, Apr. 2021.
- [29] G. E. Hinton and S. Roweis, “Stochastic Neighbor Embedding,” in *Advances in Neural Information Processing Systems*, 2002, vol. 15.
- [30] L. Gmail and G. Hinton, “Visualizing Data using t-SNE,” 2008. [Online]. Available: <https://www.jmlr.org/papers/volume9/vandermaaten08a/vandermaaten08a.pdf?fbcl>. [Accessed: 23–Jul–2023].
- [31] J. N. Acosta, G. J. Falcone, P. Rajpurkar, and E. J. Topol, “Multimodal biomedical AI,” *Nat. Med.*, vol. 28, no. 9, pp. 1773–1784, Sep. 2022.
- [32] J. Y. Koh, D. Fried, and R. Salakhutdinov, “Generating Images with Multimodal Language Models,” *arXiv [cs.CL]*, 26–May–2023.
- [33] C. Dwork, “Differential Privacy: A Survey of Results,” in *Theory and Applications of Models of Computation*, 2008, pp. 1–19.

APPENDIX

Categorical variables

last.status, age.splits, gender.concept.name, visit.concept.name, is_icu, was_ventilated, Acute.Hepatic.Injury.. during.hospitalization., Acute.Kidney.Injury..during.hospitalization., Urine.protein, kidney_replacement_therapy, kidney_transplant, htn_v, dm_v, cad_v, hf_ef_v, ckd_v, malignancies_v, copd_v, other_lung_disease_v, acei_v, arb_v, antibiotics_use_v, nsaid_use_v, smoking_status_v, cough_v, dyspnea_admission_v, nausea_v, vomiting_v, diarrhea_v, abdominal_pain_v, Microscopic_hematuria.above2, therapeutic.exnox.Boolean

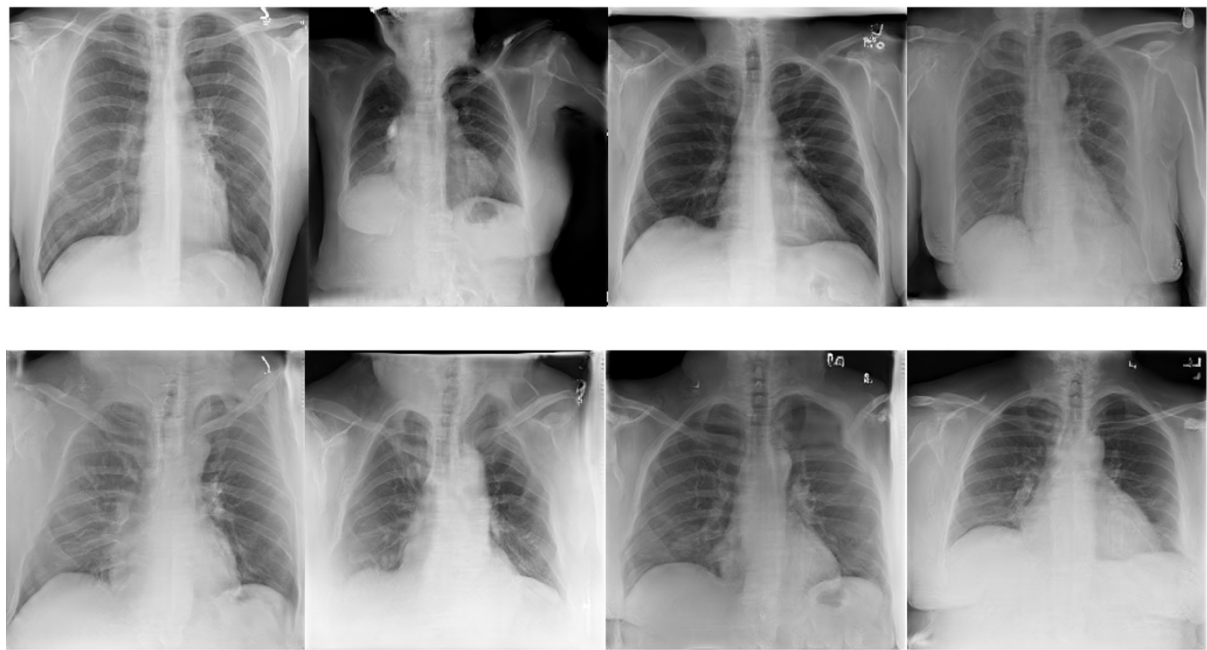
Numeric variables

invasive_vent_days, length_of_stay, days_prior_sx, Oral temperature, Oxygen saturation in Arterial blood by Pulse oximetry, Respiratory rate, Heart rate.beat-to-beat by EKG, Systolic blood pressure, Mean blood pressure by Noninvasive, Leukocytes [#/volume] corrected for nucleated erythrocytes in Blood by Automated count, Neutrophils [#/volume] in Blood by Automated count, Lymphocytes [#/volume] in Blood by Automated count, Aspartate aminotransferase [Enzymatic activity/volume] in Serum or Plasma, Alanine aminotransferase [Enzymatic activity/volume] in Serum or Plasma by No addition of P-5'-P, Creatine kinase [Enzymatic activity/volume] in Serum or Plasma, Lactate [Moles/volume] in Serum or Plasma, Troponin T.cardiac [Mass/volume] in Serum or Plasma, Natriuretic peptide.B prohormone N-Terminal [Mass/volume] in Serum or Plasma, Procalcitonin [Mass/volume] in Serum or Plasma by Immunoassay, Fibrin D-dimer DDU [Mass/volume] in Platelet poor plasma by Immunoassay, Ferritin [Mass/volume] in Serum or Plasma, reactive protein [Mass/volume] in Serum or Plasma, Hemoglobin A1c/Hemoglobin.total in Blood, Body mass index (BMI) [Ratio], Sodium [Moles/volume] in Serum or Plasma, Potassium [Moles/volume] in Serum or Plasma, Chloride [Moles/volume] in Serum or Plasma, Bicarbonate [Moles/volume] in Serum or Plasma, Urea nitrogen [Mass/volume] in Serum or Plasma, Creatinine [Mass/volume] in Serum or Plasma, Glomerular filtration rate/1.73 sq M.predicted [Volume Rate/Area] in Serum, Plasma or Blood by Creatinine-based formula (CKD-EPI), pH of Arterial blood adjusted to patient's actual temperature, Erythrocyte sedimentation rate, Glucose [Mass/volume] in Serum or Plasma, Cholesterol in LDL [Mass/volume] in Serum or Plasma by calculation, Cholesterol in VLDL [Mass/volume] in Serum or Plasma by calculation, Triglyceride [Mass/volume] in Serum or Plasma, Cholesterol in HDL [Mass/volume] in Serum or Plasma

Appendix 1. List of the 70 tabular data features used in our study. Please also refer to the information provided in the original dataset. <https://wiki.cancerimagingarchive.net/pages/viewpage.action?pageId=89096912>

Generator Layer	Activation	Output shape	Encoder Layer	Activation	Output shape
(Latent vector)		128	(Input Image)		256 × 256 × 1
Linear	LReLU	4 × 4 × 512	Convolution 1 × 1	LReLU	256 × 256 × 8
Upsampling		8 × 8 × 512	Convolution 3 × 3	LReLU	256 × 256 × 16
Convolution 3 × 3	LReLU	8 × 8 × 256	Downsampling		128 × 128 × 16
Upsampling		16 × 16 × 256	Convolution 3 × 3	LReLU	128 × 128 × 32
Convolution 3 × 3	LReLU	16 × 16 × 128	Downsampling		64 × 64 × 32
Upsampling		32 × 32 × 128	Convolution 3 × 3	LReLU	64 × 64 × 64
Convolution 3 × 3	LReLU	32 × 32 × 64	Downsampling		32 × 32 × 64
Upsampling		64 × 64 × 64	Convolution 3 × 3	LReLU	32 × 32 × 128
Convolution 3 × 3	LReLU	64 × 64 × 32	Downsampling		16 × 16 × 128
Upsampling		128 × 128 × 32	Convolution 3 × 3	LReLU	16 × 16 × 256
Convolution 3 × 3	LReLU	128 × 128 × 16	Downsampling		8 × 8 × 256
Upsampling		256 × 256 × 16	Convolution 3 × 3	LReLU	8 × 8 × 512
Convolution 3 × 3	LReLU	256 × 256 × 8	Downsampling		4 × 4 × 512
Convolution 1 × 1	Tanh	256 × 256 × 1	Linear		128
Discriminator Layer	Activation	Output shape	Code Discriminator Layer	Activation	Output shape
(Input Image)		256 × 256 × 1	(Latent vector)		128
Convolution 1 × 1	LReLU	256 × 256 × 8	Linear		1500
Convolution 3 × 3	LReLU	256 × 256 × 16	Linear		1
Downsampling		128 × 128 × 16			
Convolution 3 × 3	LReLU	128 × 128 × 32			
Downsampling		64 × 64 × 32			
Convolution 3 × 3	LReLU	64 × 64 × 64			
Downsampling		32 × 32 × 64			
Convolution 3 × 3	LReLU	32 × 32 × 128			
Downsampling		16 × 16 × 128			
Convolution 3 × 3	LReLU	16 × 16 × 256			
Downsampling		8 × 8 × 256			
Convolution 3 × 3	LReLU	8 × 8 × 512			
Downsampling		4 × 4 × 512			
Linear		1			

Appendix 2. The α GAN architecture in our study.



Appendix 3. The relationship between BMI and Chest X-ray images (CXR). The upper row shows normal cases with BMI ranging from 18.5 to 25, and the lower row shows morbidly obese cases with BMI over 40. All were randomly selected from sDB. This shows that the lower rows generally have thicker subcutaneous fat. It is evident that the thickness of subcutaneous fat is generally greater in the bottom row compared to the top row, suggesting that the correspondence between CXR and BMI is maintained.